

Characterization and Synthesis of CdO and CdO_{1-x}:S_x Films by Pulsed Laser Deposition

Omar A. Thuhaib* and Hassan Hashim

Department of Physics, College of Science, Al-Nahrain University, Baghdad-Iraq

Article's Information

Received:
15.09.2021
Accepted:
01.11.2021
Published:
31-12-2021

Keywords:

LIP
CdO
CdO:S thin films
XRD
AFM and optical UV-VIS

Abstract

In this work, we analyze the effects of S doping on the structural and optical characteristics of pure cadmium oxide (CdO) films at varying concentrations of CdO_{1-x}:S_x (X = 0.2, 0.4, and 0.6), Sulfur is a chemical element with the atomic number 16 and the symbol S. The films were created using a laser-induced plasma (LIP) with a wavelength of 1064 nm and a duration of 9 ns at a pressure of 2.5×10^{-2} mbar. X-ray diffraction studies revealed that all of the produced films are polycrystalline. The topography of the film's surface was evaluated using AFM, and the findings revealed that as the amount of doping increases, so does the grain size, along with an increase in the average roughness. The absorbance spectrum of the wavelength range (350-1100) nm was used to investigate the optical characteristics of all films. This rise might be the so-called Borsstein-Moss displacement has been viewed as a result of this. because the lowest layers of the conduction beams are densely packed with Because electrons require more energy to move, it seems as though the energy disparity widens.

DOI: 10.22401/ANJS.24.4.04

*Corresponding author: omar.duheeb92@gmail.com

1. Introduction

In many technical settings, the pulse laser deposition method is one of the best and cheapest procedures for semiconductor and mineral deposits and oxides. Despite the fact that pulse laser deposition was initially utilized in the production of thin films in 1960 [1]. To precipitate a thin layer from a single target, pulse laser deposition (PLD) is typically used. PLD uses high-intensity laser pulses with an energy density of greater than 10^8 (W/cm²). Because this sort of semiconductor material is often produced as thin films [2]. The vapor develops a thick layer over the surface of the target material in the primitive portion of the pulsed laser, leading to energy absorption and an increase in pressure in addition to the temperature of this vapor, resulting in partial ionization. Due to the high pressure, this layer will extend beyond the intended surface. This is referred as plasma plume [3]. Due to their excellent optical transmittance and low resistance, thin films of conductive oxide (TCO) such as cadmium oxide, zinc oxide, Tin oxide, and copper oxide are highly regarded [4]. Cadmium oxide is a semiconducting substance that has a wide range of applications. It possesses a number of physical characteristics, including transparency, a high absorption coefficient, and a relatively big energy gap; as a result, it's utilized in a variety of optical and electrical applications, as well as a variety of significant industrial applications that have helped to progress modern technology and science, such as cells, optical and solar reagents [5]. The study aimed

to investigate in the synthesis of CdO films by pulsed laser deposition at different concentrations.

2. Experiment Part

The pure cadmium oxide material supplied by the German business (FLUKA) was utilized to make the pure cadmium oxide films, which had a purity of (99.9%), as well as the creation of a cadmium oxide film impregnated with sulfur by adding pure sulfur (S) manufactured by the same business and having a purity (99.8%). A pulsed laser deposition technique was used to create thin films. where pulses with (E = 360) mJ were directed from a Nd:YAG laser with a wavelength of (1064) nm, a frequency of (6) Hz, and a duration of (9) ns in vacuum (2.5×10^{-2}) mbar. The experimental configuration of (PLD) as shown in Figure 1.

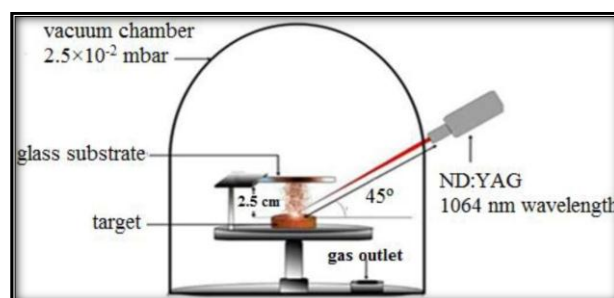


Figure 1. Schematic diagram of pulsed laser deposition (PLD) experiment [6].

The number of pulses, the pulse energy, and the size of the laser spot may all be regulated and varied depending on the distance between the laser lens and the target. The laser beam was focused on the target and formed a 45-degree angle with it. typically 2 gm implies a pellet thickness of 15 mm, which is CdO and CdO_{x-1}: S_x at (X = 0.2, 0.4 and 0.6) was crushed with a hydraulic piston at 6.8 bar pressure to produce a disc with a thickness of 4.0 cm and a diameter of 1 cm. An X-ray diffraction apparatus with an X-ray emitter type Cu (K α), wavelength = 1.5418 Å, energy = 30 KV, current = 10 mA was used to examine the crystal structure of all films. The morphological features of nano films CdO and CdO_{1-x}: S_x at (X = 0.2, 0.4 and 0.6) produced on a glass slide using the (PLD) method were studied using atomic force microscopy (AFM). A double beam UV-Vis spectrophotometer (Metertech SP8001, Taiwan) was used to investigate the optical characteristics. Within the spectrum range of 100-1100, the absorption spectra of the produced NPs were investigated under various circumstances. Using a graph, the optical band gap was calculated from direct transitions, Tauc's relationship applies [7].

$$(ahv)^2 = A(hv - E_g) \quad \dots(1)$$

where A is constant, h is plank's constant, v is incoming photon frequency, E_g is optical energy gap, and n is a constant dependent on the type of the transition.

3. Results and Discussion

3.1 X-ray diffraction examination:

X-ray diffraction (XRD) was used to calculate the crystalline structure and grain size of the CdO and CdO_{x-1}: S_x films prepared by PLD techniques. D was the grain size. Scherer's equation was used to compute it [8].

$$D = \frac{k\lambda}{\beta \cos \theta} \quad \dots(2)$$

where k is a constant taken to be 0.94, λ is the wavelength of X-ray 1.54 Å, β is full width at half maximum (FWHM), and θ is Bragg's angle [9].

Figure 2 displays the XRD patterns for CdO powder, which indicate that the material has a cubic structure with diffraction peaks at crystalline hkl (111), (200), (220), (311), and (222) which correspond to $2\theta = 33.05, 38.35, 55.35, 65.95,$ and 69.25 respectively. The results are in good agreement with the provided data's standard values (JCPDS No. 96-900-6674). The structural diagram is shown in Table 1. The Bragg angle (2θ), full width half maxima (FWHM), and other characteristics for CdO powder, Scherrer's equation was used to determine the experimental inter plane gap and crystalline size.

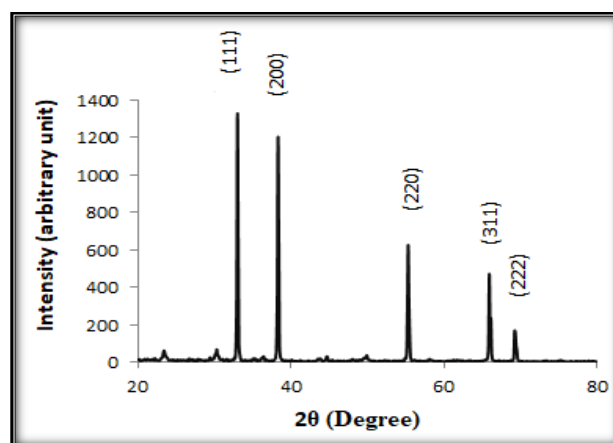


Figure 2. X-ray pattern of CdO Powder [6].

Table 1. XRD for the CdO powder in comparison with the standard [6].

Sample	2θ (Deg.)	FWHM (Deg.)	C.S (nm)	d _{hkl} Exp.(Å)	d _{hkl} Std. (Å)	hkl	Card No.
CdO	33.05	0.2952	28.1386	2.7095	2.707	(111)	96-900-6674
	38.35	0.2952	28.5583	2.3467	2.345	(200)	96-900-6674
	55.35	0.2952	30.4457	1.6591	1.658	(220)	96-900-6674
	65.95	0.2952	32.1283	1.4150	1.414	(311)	96-900-6674
	69.95	0.2952	32.8878	1.3550	1.172	(222)	96-900-6674

X-ray diffraction of the CdO and CdO_{x-1}: S_x thin films of thickness 200 nm, at (X = 0.2, 0.4 and 0.6), are shown in the Figure 3. With peaks appearing at $2\theta = 33.05, 38.35, 55.35$ and 65.95 , belong to hkl [(111), (200), (220) and (311)] of the material, which identical with (JCPDS) card No. (5-0540), as well as the appearance of peaks in the directions (222) and (040) at $2\theta = 22.5$ and 26.49 of the material (S) Which identical with (JCPDS) card No. (08-0274). where it is observed with an increase in the doping, crystal growth begins Clearly, crystallization is improving and the appearance of peaks indicates that the structure of

the sedimentary models is a polycrystalline structure due to the presence of more than one peak and a cubic structure. The Table 2 shows the diffraction angles, mid-peak width and crystal size of the models at each deposition energy, E = 300 mJ.

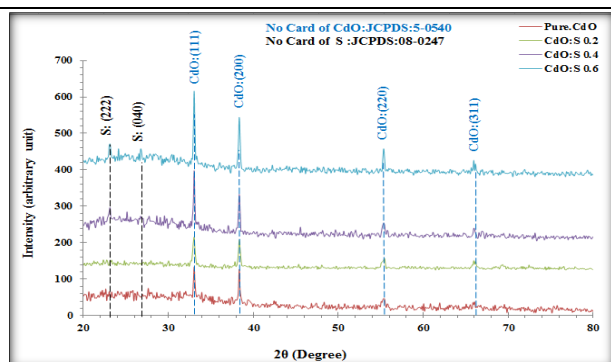


Figure 3. X-ray diffraction pattern for CdO and $(\text{CdO}_{1-x} : \text{S}_x)$ films.

Table 2. Structural parameters of CdO and $(\text{CdO}_{x-1} : \text{S}_x)$ films obtained from (XRD) examination.

Sample	2θ (Deg.)	FWHM (Deg.)	C.S (nm)	Avg. C.S (nm)	hkl	Card No.
CdO	33.08	0.5904	14.024	19.52339	(111)	96-900-6674
	38.37	0.2952	28.3292		(200)	96-900-6674
	55.35	0.7231	11.8371		(220)	96-900-6674
	65.95	0.2813	32.2086		(311)	96-900-6674
	69.95	0.8310	11.2181		(222)	96-900-6674
CdO:S (0.2)	33.05	0.2952	28.0481	21.89271	(111) CdO	JCPDS:05-0540
	38.36	0.2952	28.3292		(200) CdO	JCPDS:05-0540
	55.34	0.492	17.3996		(220) CdO	JCPDS:05-0540
	65.99	0.642	14.1126		(311) CdO	JCPDS:05-0540
	69.75	0.4321	21.5742		(222) CdO	JCPDS:05-0540
CdO:S (0.4)	23.31	0.423	19.574	27.96	(222) S	JCPDS:08-0247
	26.98	0.231	36.3598		(026) S	JCPDS:08-0247
	33.03	0.2952	28.0481	23.94008	(111) CdO	JCPDS:05-0540
	38.36	0.2952	28.3292		(200) CdO	JCPDS:05-0540
	55.34	0.492	17.3996		(220) CdO	JCPDS:05-0540
	65.98	0.5341	16.9637		(311) CdO	JCPDS:05-0540
	69.95	0.3219	28.9599		(222) CdO	JCPDS:05-0540
CdO:S (0.6)	23.31	0.482	17.178	19.89744	(222) S	JCPDS:08-0247
	26.98	0.2931	28.5321		(026) S	JCPDS:08-0247
	28.96	0.5981	13.9822		(040) S	JCPDS:08-0247
	33.03	0.2952	28.0481	24.28777	(111) CdO	JCPDS:05-0540
	38.36	0.2952	28.3292		(200) CdO	JCPDS:05-0540
	55.34	0.5904	14.4996		(220) CdO	JCPDS:05-0540
	65.98	0.4210	21.5209		(311) CdO	JCPDS:05-0540
	69.95	0.3210	29.0411		(222) CdO	JCPDS:05-0540

3.2 The absorption coefficient:

In all films of pure cadmium oxide and doped with sulfur $\text{CdO}_{1-x} : \text{S}_x$ ($X = 0.2, 0.4$ and 0.6), at laser energy $E = 300$ mJ, the absorption coefficient (α) changes as a function of wavelength, as seen in Figure 4. The results revealed that

increasing the doping ratio resulted in a significant increase in all absorption coefficient values, for the state revaccination. Because donor levels are generated within the energy gap close to the conduction band [10,11].

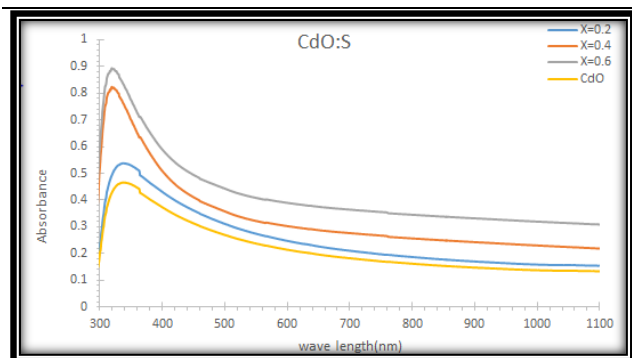


Figure 4. Variation of absorption coefficient as a function of wavelength for pure CdO and $CdO_{1-x}S_x$ ($X = 0.2, 0.4$ and 0.6).

3.3 Calculation of the optical energy gap (E_g):

The optical energy gap is critical in determining the extent to which thin films generated in the manufacturing of hybrid joints, reagents, and solar cells may be used. When there is a graphical representation of the relationship between $(\alpha h\nu)^2$ was drawn as a function of the photon energy ($h\nu$), as in Figure 5. where the value of the direct visual energy gap is represented by the intersection of the straight part of the curve with the photon energy axis ($\alpha h\nu^2 = 0$). Figure 5 shows the optical energy gap for direct permissible transport of CdO and $CdO_{1-x}S_x$ films, and shows the optical energy gap for direct allowable transport of CdO and $CdO_{1-x}S_x$ films, at $X = 0.2, 0.4$ and 0.6 .

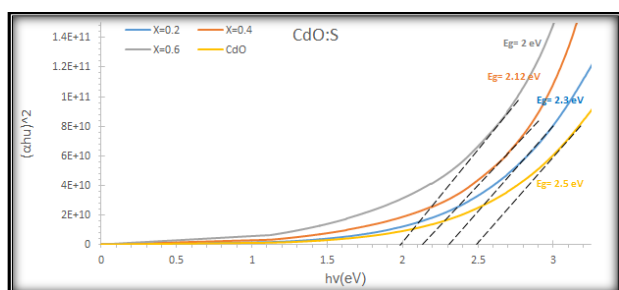


Figure 5. The variation of $(\alpha h\nu)^2$ versus photon energy ($h\nu$) for CdO and $CdO_{1-x}S_x$ thin films deposited on glass substrate.

The energy gap for the permissible direct transmission of a membrane (CdO), according to the findings (2.5 eV), the value of the absorption coefficient is thus equal to ($\alpha \geq 10^2$), confirming that the energy gap is a direct gap, and this conclusion is consistent with previous study findings. Within different preparation techniques [12,13], the increase of CdO content leads to a decrease in the optical bandgap. The decreasing of E_g with the increasing CdO content may be due to an increase in particle size. All values are tabulated in Table 3.

Table 3. The energy gap of CdO pure and $CdO_{1-x}S_x$ for ($X = 0.2, 0.4$ and 0.6) deposited.

Sample	E_g (Ev)
CdO	2.5
CdO:S (0.2)	2.3
CdO:S (0.4)	2.12
CdO:S (0.6)	2

3.4 Atomic force microscope:

Atomic force microscope (AFM) pictures of a system where pure CdO and the various doping ratio $CdO_{1-x}S_x$ were investigated are shown Figures 6 (a- pure CdO, b- $X = 0.2$, c- $X = 0.4$ and d- $X = 0.6$). Where the development of semi-spherical clusters and closer average diameter was seen when smooth surfaces and high-quality adherence to the glass substrate were present. The nanostructure's surface is caused by a rise in the percentage of scraping which results in an increase in the granular size, as shown in Table 4. This region is free of particles. During the deposition process, the layers of the nanostructure reach the surface via the interaction of ions and uncharged ablation fractions. The energy of rapid ions is shown by the fragments and the speed of the uncharged ions is associated with the number of collisions. The result is an increase in the probability of larger granules being created during a high-energy skimming or excision, which in turn increases the roughness of the nanostructure surface. An example of this was found in the atomic force microscopy findings. The findings of agreement with the findings of this article [8].

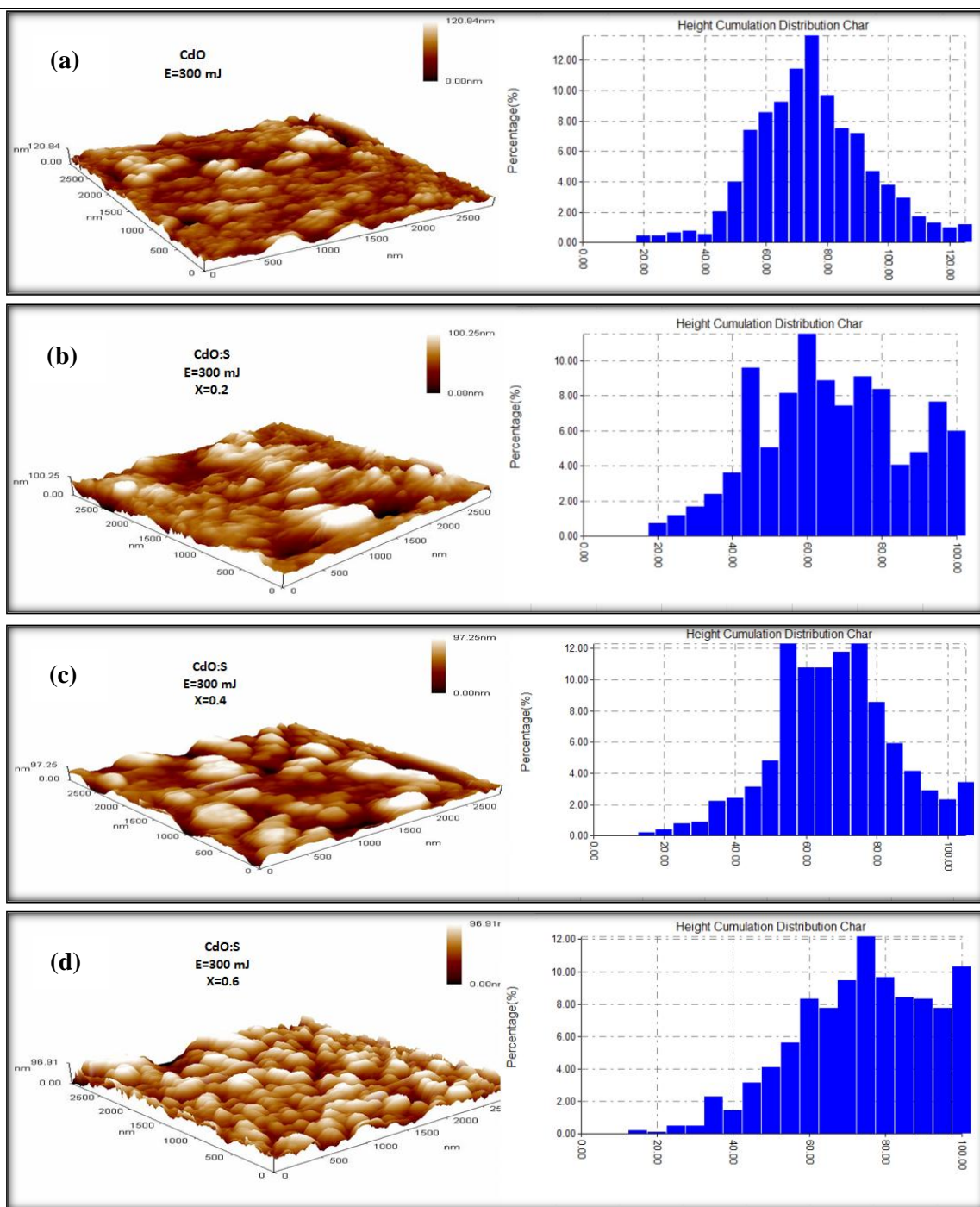


Figure 6. AFM images of CdO and CdO_{1-x}S_x thin films deposited with different S concentration at (X = 0.2, 0.4 and 0.6).

Table 4. Structural parameters of CdO and CdO_{1-x}S_x membranes obtained from the AFM examination.

Laser energy = 300 (mJ)				
Sample	Ratio	Avg. Diameter(nm)	Root Mean Sq. (nm)	Ave. Roughness (nm)
CdO:S	X = 0.2	64.1	19.6	15.2
	X = 0.4	65.4	21.8	17.8
	X = 0.6	71.5	28.9	21.2
CdO	Pure	72.6	20.8	16

4. Conclusion

The $\text{CdO}_{1-x}\text{S}_x$ film was prepared using an Nd:YAG laser with a fundamental wavelength of 1064 nm. on the glass substrate. The X-ray findings revealed that all thin films are polycrystalline and have a cubic structure with direction dominance (111). The results of AFM show that the higher the percentage of doping, the increase in grain size. As for the properties measurements, it was found that the absorption coefficient increase as the percentage of doping increases. Whereas the energy gap, on the other hand, decreases with the rate of doping increases.

Reference

- [1] Ashfold M. N. R.; Claeysens F.; Fuge G. M. and Henley S. J.; *Chemical Society Reviews*, 33: 23-31, 2004.
- [2] Gunasekara M. and Ichimura M.; *Japanese Journal nanocrystals*, 376, 659-663, 2011.
- [3] Eason R.; "Pulse Laser Deposition of Thin Films", University of Southampton, UKA John Wiley and Sons, INC.; 2007.
- [4] Aksoy S.; Caglar Y.; Ilcan S. and Caglar M.; *International Journal of Hydrogen Energy*, 34(12): 5191-5195, 2009.
- [5] Lazem H. G.; *Journal of Missan Researches*, 2-4, 2006.
- [6] Wadaa S. H.; Ala' F. A. and Kadhim A. A.; "Influence of Laser Energy and Annealing on Structural and Optical Properties of CdS Films Prepared by Laser Induced Plasma". Department of Physics, College of Science, University of Baghdad, 2019.
- [7] Venkata R.; Ch. R.; Ganganagunta R. S.; Jaesool S. and Migyung Ch.; "Structural, optical, and improved photocatalytic properties of CdS/SnO₂ hybrid photo catalyst nanostructure", *Materials Science and Engineering, B*, 221: 63-72, 2017.
- [8] Al-Douri, Y.; Fakhri, M. A.; Badi, N. and Voon C. H.; "Effect of stirring time on the structural parameters of nano photonic LiNbO₃ deposited by spin-coating technique," *Optik (Stuttg)*, 156(12): 886-890, 2018.
- [9] Mohammed K.; Baha T.; Ala' F. and Falah A-H. 2013. "Thin film technique for preparing nanoZno gas sensing (O₂, No₂) using plasma deposition", *Int. J. Appl. Innov. Eng. Manag* 2: 178-184, 2013.
- [10] Hassan K. and *Electrochem J. Sci.*; 5, 720-730, 2010.
- [11] Jasim M. H.; Awatif S. J. and Kadhim A. A.; "Synthesis and Characterization of $\text{CdO}_{x-1} : \text{Mg}_x$ films by pulsed laser deposition", Department of Physics, College of Sciences, University of Baghdad, Iraq, 2020.
- [12] Bhosale C. H. and Kambale A. V.; *Materials Science and Engineering, B122*: 67-71, 2005.
- [13] Amrut S. L.; *Indian Journal of Pure and Applied Physics*, 49, 234-238, 2011.